



Dynamic stability enhancement of interconnected multi-source power systems using hierarchical ANFIS controller-TCSC based on multi-objective PSO

Ali Darvish FALEHI[†], Ali MOSALLANEJAD

(Department of Electrical Engineering, Shahid Beheshti University, Tehran 1983963113, Iran)

[†]E-mail: a_darvishfalehi@sbu.ac.ir

Received Sept. 30, 2015; Revision accepted Mar. 13, 2016; Crosschecked Jan. 20, 2017

Abstract: Suppression of the dynamic oscillations of tie-line power exchanges and frequency in the affected interconnected power systems due to loading-condition changes has been assigned as a prominent duty of automatic generation control (AGC). To alleviate the system oscillation resulting from such load changes, implementation of flexible AC transmission systems (FACTSs) can be considered as one of the practical and effective solutions. In this paper, a thyristor-controlled series compensator (TCSC), which is one series type of the FACTS family, is used to augment the overall dynamic performance of a multi-area multi-source interconnected power system. To this end, we have used a hierarchical adaptive neuro-fuzzy inference system controller-TCSC (HANFISC-TCSC) to abate the two important issues in multi-area interconnected power systems, i.e., low-frequency oscillations and tie-line power exchange deviation. For this purpose, a multi-objective optimization technique is inevitable. Multi-objective particle swarm optimization (MOPSO) has been chosen for the optimization problem, owing to its high performance in untangling non-linear objectives. The efficiency of the suggested HANFISC-TCSC has been precisely evaluated and compared with that of the conventional MOPSO-TCSC in two different multi-area interconnected power systems, i.e., two-area hydro-thermal-diesel and three-area hydro-thermal power systems. The simulation results obtained from both power systems have transparently certified the high performance of HANFISC-TCSC compared to the conventional MOPSO-TCSC.

Key words: Hierarchical adaptive neuro-fuzzy inference system controller (HANFISC); Thyristor-controlled series compensator (TCSC); Automatic generation control (AGC); Multi-objective particle swarm optimization (MOPSO); Power system dynamic stability; Interconnected multi-source power systems

<http://dx.doi.org/10.1631/FITEE.1500317>

CLC number: TM76; TP391

1 Introduction

During the last decade, extensive and sequential development of electrical power systems in size and complication, along with the expansion of interconnected power systems, has become an important and complex issue for dynamic stability, power quality, protection systems, and the like (Iracleous and Alexandridis, 2005; Kazemi *et al.*, 2007; Bevrani *et al.*, 2008; Tan and Xu, 2009). Dynamic behavior of a power system depends strongly on the operation

conditions and load perturbation, which accordingly can exacerbate the oscillations' amplitude and loss of synchronism (Falehi *et al.*, 2012; Abd-Elaziz and Ali, 2015; Abd-Elazim and Ali, 2016). Automatic generation control (AGC) aims at untangling these problems. Generally, in every area of an interconnected power system, the AGC system detects the frequency and tie-line power exchanges, elicits the net changes in the generation, and accordingly regulates the set conditions of the generators through these areas (Ali and Abd-Elazim, 2011; 2013). Its accurate and safe operation involves an acceptable alleviation of the system frequency and tie-line power exchange deviations during load perturbation events (Kundur *et al.*,

ORCID: Ali Darvish FALEHI, <http://orcid.org/0000-0002-8333-0114>

© Zhejiang University and Springer-Verlag Berlin Heidelberg 2017

1989). It can be stated that an AGC system tracks three principal targets in interconnected multi-source power systems:

1. canceling the steady-state errors of system frequency deviations,
2. achieving good tracking performance without persistent oscillations during load disturbances, and
3. abating dynamic oscillations of tie-line power and frequency deviation.

Future outlook in the competitive electricity market, heterogeneous species of equipment with a wide range of capacities, and fast power consumption can give rise to intense disturbance due to frequency oscillations. In case of non-availability of sufficient damping, these system frequency oscillations would lie within the inter-area oscillation mode (0.2–0.8 Hz), which can be maintained and intensified until the instability problem occurs (Kundur *et al.*, 1989; Falehi *et al.*, 2012). Therefore, many researchers have dealt with the competency of flexible AC transmission system (FACTS) devices, aimed at the effective control of power systems. Because of the better flexibility of these devices, they not only augment the power transfer capability of transmission lines, but also enhance the dynamic stability of the power system (Gyugyi, 1992; Larsen *et al.*, 1995; Chaudhuri *et al.*, 2003; Chaudhuri and Pal, 2004; Cai and Erlich, 2005; Falehi *et al.*, 2011; Falehi, 2012).

Thyristor-controlled series compensator (TCSC) is one kind of series FACTS devices recognized as effective and economical to suppress power system oscillations, enhance transient stability, alleviate sub-synchronous resonance (SSR), and restrict short-circuit currents (Mattavelli *et al.*, 1997; Li *et al.*, 2000; del Rosso *et al.*, 2003; Falehi, 2012). A conventional multi-objective particle swarm optimization-TCSC (MOPSO-TCSC) has been constructed by a permanent series capacitor, which is shunted by a thyristor-controlled reactor (TCR). Generally, TCR is composed of a reactor in series with a bidirectional thyristor fired by a phase angle (between $\pi/2$ and π) in accordance with the capacitor's voltage. The reactance of TCSC is tuned directly by the thyristor's firing angle (Benabid *et al.*, 2009; Soliman *et al.*, 2011). By definition, occurrence of various disturbances in a power system would have special responses that may lead to instability. Therefore, it is absolutely essential that a high-performance controller be chosen

for TCSC aimed at bringing back the power system to the stable status.

Recently, fuzzy controllers have been widely and successfully implemented in a number of nonlinear systems whose behavior is extremely intricate to model (Karnavas and Papadopoulos, 2000; Elshafei *et al.*, 2005; Moradi *et al.*, 2014). Power systems are such nonlinear systems; thus, the application of an effective controller based on a fuzzy-logic controller (FLC) can be regarded as a good solution. Based on the benefits of both FLC and artificial neural network (ANN), the best strategy to construct a powerful processing tool is incorporating them, whereby an adaptive neuro-fuzzy inference system (ANFIS) is realized. In fact, ANFIS combines the self-learning capability of ANN with the linguistic expression function of fuzzy inference (Zhang *et al.*, 2008).

Currently, one of the most significant issues in the field of fuzzy systems is how to bring down the number of included rules along with the relevant computational requirements. In the conventional fuzzy controllers, the number of rules has exponentially grown while the elicited results are hardly precise or explainable. As an example, for n input variables and membership function, rules would be essential to set out a fuzzy controller. According to the mentioned relationship, the rule base will rapidly occupy the memory by increasing n , which may make it difficult to apply the fuzzy controller. One practical strategy to avoid this problem is set out the input variables hierarchically (Raju *et al.*, 1991; Benítez and Casillas, 2013). A hierarchical fuzzy-rule-based system (HFRBS) is composed of a number of low-dimensional hierarchical fuzzy systems. This strategy will lead to a linear growth of the total number of rules, less computational effort, and high reliability of the fuzzy controller (Kikuchi *et al.*, 1998; Lee *et al.*, 2003). Eventually, this results in the hierarchical ANFIS controller-TCSC (HANFISC-TCSC) to augment the power system dynamic stability.

Moreover, being a multi-objective problem, it is imperative that an effective multi-objective optimization technique should be used. This is because a single objective function with contribution from several cost functions accompanied by relevant weights cannot certainly untangle the problem under study. Therefore, the MOPSO technique is selected to solve the optimization problem. For this study, two different multi-area interconnected power systems, i.e.,

two-area hydro-thermal-diesel and three-area hydro-thermal power systems, have been selected to test and evaluate the proficiency of HANFISC-TCSC. The occurrence of step load perturbation (SLP) affects the aforementioned power systems, so the efficiency and robustness of HANFISC-TCSC need to be evaluated. To overcome the uncertainty in the controller's parameters against different perturbations in all the areas of both power systems, a simultaneous optimization scheme is proposed in this study. In other words, SLP is assumed to occur in all areas of both interconnected multi-source power systems, and the simultaneous optimization scheme is subsequently settled. Meanwhile, a conventional MOPSO-TCSC is evaluated alongside HANFISC-TCSC to better demonstrate the efficiency of the latter. In the long run, simulation results have transparently ascertained the superior performance of HANFISC-TCSC compared to the conventional MOPSO-TCSC in both multi-area interconnected power systems.

Table 1 gives the notations used in this paper.

2 Description of the multi-objective particle swarm optimization technique

2.1 MOPSO review

PSO is a stochastic global optimization technique based on the simulation of the social deportment of birds and fish into their flock. In PSO, each particle of the swarm regulates its trajectory in accordance with its own flight experience and the other particles' flying experience by juxtaposition in the search space (Hingorani and Gyugyi, 2000; Eberhart *et al.*, 2001). In this study, the procedure of optimization has more than one objective, and thus enforcement of multi-objective optimization is obligatory. Generally, the multi-objective alternative of a problem is more difficult than the single-objective problem. The interaction of these objectives yields a set of effective solutions known as Pareto-optimal solutions, which provide a determinant more flexibility in the engagement of an appropriate alternative.

Table 1. Nomenclature			
Notation	Description	Notation	Description
AGC	Automatic generation control		Speed deviation of the i th machine
TCSC	Thyristor-controlled series compensator	T_1, T_2, T_3, T_4	Lead lag block time constants
HANFISC	Hierarchical adaptive neuro-fuzzy inference system controller	K_{TCSC}	TCSC controller's gain
MOPSO	Multi-objective particle swarm optimization	T_{TCSC}	TCSC controller's time constant
SLP	Step load perturbation	GRC	Generation rate constraint
FACTS	Flexible AC transmission system	ACE	Area control error
HFRBS	Hierarchical fuzzy rule-based system	B_i	Frequency bias coefficient of the i th area
$f(\mathbf{X})$	Objective function's vector	a_{12}, a_{13}, a_{23}	Ratios of areas' power ratings
\mathbf{X}	Variables' vector	R	Governor regulation
g_i, h_j	Problem's constraint functions	T_g	Governor time constant
F	Feasible region	T_i	Non-reheat time constant
P^*	Pareto optimal front	T_r	Reheat time constant
c_1, c_2	Global learning coefficients	Δf_i	Frequency error of the i th area
φ_1, φ_2	Acceleration constants	ΔP_{Di}	Incremental load change in area i
φ	Mathematical function of acceleration constants	$\Delta P_{tie, i, j}$	Tie-line power deviation between the i th area and the j th area
iter	Iteration index	t_{sim}	Time range of the simulation
W_{max}, W_{min}	Final weight and initial weight	N_p	Number of SLPs
FIS	Fuzzy inference system	K_{ef}, K_{def}	HANFISC-TCSC controller's gains
A_i	Linguistic label	K_{uf}, K_{dep}, K_u	
θ_c	Angle of the current	F_f	Objective function related to the low-frequency power oscillations
ΔI	Supplemental current	F_p	Objective function related to the tie-line power exchange deviations
k_c	Rate of compensation		
T_{mn}^0	Synchronizing coefficient		
$\Delta P_{mn}, \Delta Q_{mn}$	Active and reactive power flow with TCSC		

2.2 Basic concepts of multi-objective functions

The problem's solution can be mathematically presented as follows:

Find X which optimizes

$$f(X) = [f_1(X), f_2(X), \dots, f_k(X)] \quad (1)$$

subject to

$$g_i(x) \leq 0, i = 1, 2, \dots, m, \quad (2)$$

$$h_j(x) \leq 0, j = 1, 2, \dots, p, \quad (3)$$

where $X = [X_1, X_2, \dots, X_n]^T$ is the decision variable vector, $f_i(\cdot)$ ($i = 1, 2, \dots, k$) are the objective functions, and $g_i(\cdot)$ and $h_j(\cdot)$ are the problem's constraint functions.

In fact, multi-objective optimization problems are aimed at attaining good compromises. To perceive the concept of Pareto optimality, some definitions have been introduced:

Definition 1 Provided two vectors $X, Y \in \mathbb{R}^n$, which can be cited that $X \leq Y$ if $x_i \leq y_i$ for $i = 1, 2, \dots, k$, then X dominates Y (indicated by $X \prec Y$) if $X \leq Y$ and $X \neq Y$.

Definition 2 A decision variable vector $X \in \chi \subset \mathbb{R}^n$ is non-dominated regarding χ , if there is no $X' \in \chi$ such that $f(X') \prec f(X)$.

Definition 3 A decision variable vector $X^* \in F \subset \mathbb{R}^n$ (F is the doable area) is Pareto-optimal if it is non-dominated regarding F .

Definition 4 The Pareto-optimal set P^* is determined by

$$P^* = \{X \in F \mid X \text{ is Pareto optimal}\}. \quad (4)$$

Definition 5 The Pareto front PF^* is determined by

$$PF^* = \{f(X) \in \mathbb{R}^k \mid X \in P^*\}. \quad (5)$$

2.3 PSO construction

For the proposed approach, the velocity and position of a particle are computed as follows (Panda and Padhy, 2008):

$$v_{i,d}^{(t+1)} = \psi \left[w \cdot v_{i,d}^{(t)} + c_1 + r_1(\text{pbest}_{i,d} - x_{i,d}^{(t)}) + c_2 + r_2(\text{gbest}_d - x_{i,d}^{(t)}) \right], \quad (6)$$

$$x_{i,d}^{(t+1)} = x_{i,d}^{(t)} + v_{i,d}^{(t+1)}, \quad i = 1, 2, \dots, n, d = 1, 2, \dots, m, \quad (7)$$

$$v_d^{\min} \leq v_{i,d}^{(t)} \leq v_d^{\max}, \quad (8)$$

$$\psi = \frac{2}{2 - \varphi - \sqrt{\varphi^2 - 4\varphi}}, \quad (9)$$

$$\varphi = \varphi_1 + \varphi_2, \quad \varphi > 4, \quad (10)$$

$$w = w_{\max} - \frac{w_{\max} - w_{\min}}{\text{iter}_{\max}} \cdot \text{iter}, \quad (11)$$

where c_1 and c_2 are both positive constants, called personal and global learning coefficients, respectively, r_1 and r_2 are random numbers produced from a uniform distribution in range (0, 1), $v_{i,d}^{(t)}$ is the velocity of the d th part of particle i at iteration t , $x_{i,d}^{(t)}$ is the position of the d th part of particle i at iteration t , $\text{pbest}_{i,d}$ is the personal best value of the d th part of particle i , gbest_d is the global best value of the d th part of the group, ψ is a constriction factor extracted from the stability analysis of Eq. (6) to confirm the system to converge but not precipitately, ψ is a mathematical function of φ_1 and φ_2 , which are acceleration constants, and w is the inertia weight for PSO's convergence, adjusting the impact of the prior velocities on the present velocity to find a suitably optimal solution. Likewise, iter_{\max} , iter , w_{\min} , and w_{\max} are the maximum iteration number, current iteration index, final weight, and initial weight, respectively.

2.4 Non-dominated sorting PSO principle

The algorithm carries out non-dominated sorting to retain the solutions situated in the first five fronts (Fig. 1). The procedure figures out the first particles of the non-dominated front for all of the archive's members. Whenever the front length is less than the maximum bound, the front will be retained in the archive. Therefore, to figure out the individuals in the next front, the first front's solutions are provisionally overlooked, and the above procedure is replicated till five fronts are found (Fig. 1a). Whenever the front is to be retained in the archive, it will be larger than the admissible bound and a crowding length is calculated to sieve the solutions and the following fronts will be omitted (Fig. 1b). The flowchart of the proposed algorithm is shown in Fig. 1c.

Retracted

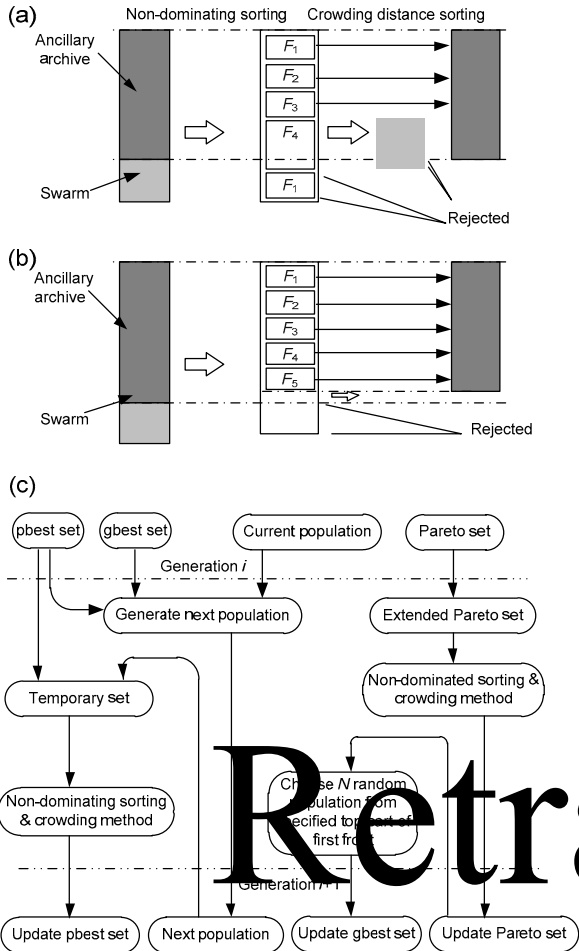


Fig. 1 Non-dominated MOPSO technique's procedure: (a) the front length is less than the maximum bound and the front will be retained in the archive; (b) the front length is larger than the maximum bound and the following fronts will be omitted; (c) the flowchart of the proposed algorithm

3 Design of TCSC by hierarchical ANFIS-type fuzzy strategy

3.1 Fuzzy logic guideline

In general, a fuzzy system is set up based on four principal structures: fuzzifier, inference engine, knowledge base, and defuzzifier. At first, the fuzzy system computations are transformed from the numeric sets into the fuzzy sets, which is called fuzzification. In fuzzy set theory, the inference engine is the heart of the fuzzy system that carries out all logic operations in the system. The knowledge base system is made up of membership functions and if-then rules (Dash *et al.*, 2004; Talaat *et al.*, 2010).

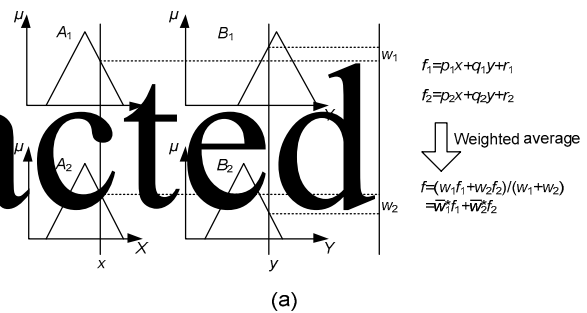
3.2 ANFIS control strategy and structure

ANFIS is a category of adaptive multi-layer feed-forward networks functionally similar to a fuzzy inference system (FIS). In fact, ANFIS acts in the same way as an adaptive network simulator of a Takagi-Sugeno type FIS. ANFIS synthesizes the self-learning capability of neural network (NN) with the fuzzy's linguistic expression function (Talaat *et al.*, 2010). In accordance with the first-order Sugeno fuzzy style, the concept of ANFIS structure with two fuzzy if-then rules can be represented as follows:

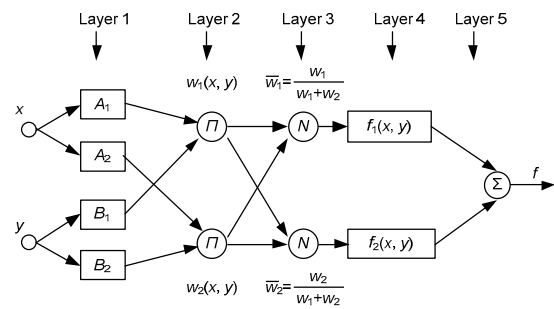
Rule 1 If x is A_1 and y is B_1 , then $f_1=p_1x+q_1y+r_1$.

Rule 2 If x is A_2 and y is B_2 , then $f_2=p_2x+q_2y+r_2$.

The fuzzy reasoning is explained in Fig. 2a, and the relevant equivalent ANFIS construction is presented in Fig. 2b.



(a)



(b)

Fig. 2 Multi-layer perception fuzzy reasoning (a) and equivalent ANFIS structure (b)

The ANFIS structure consists of five layers. Each layer incorporates a number of nodes described by the node's function. The node functions in the same layer are of the same function family and are represented as follows:

Layer 1: Each node i in this layer is indicated by a square node with a node (Fig. 2b) function:

$$O_i^1 = \mu_{A_i}(x) = \begin{cases} 0, & x \leq a_i, \\ \frac{x - a_i}{b_i - a_i}, & a_i \leq x \leq b_i, \\ \frac{c_i - x}{c_i - b_i}, & b_i \leq x \leq c_i, \\ 0, & c_i \leq x, \end{cases} \quad (12)$$

where x represents the input to node i , A_i represents the linguistic label related to this node function, O_i^1 is the membership function of A_i and defines the degree to which the presented x satisfies A_i , and a_i , b_i , and c_i comprise the parameter set. ANFIS suggests several classes of membership functions, i.e., trapezoidal, triangular, generalized bell, Π -shaped, Gaussian curve, and Gaussian combination. Commonly, $\mu_{A_i}(x)$ is selected to be triangle-shaped with its maximum equal to 1 and minimum equal to 0. Eq. (12) can be rewritten in a contracted form:

$$\mu_{A_i}(x) = \max \left(\min \left(\frac{x - a_i}{b_i - a_i}, \frac{c_i - x}{c_i - b_i} \right), 0 \right) \quad (13)$$

When changing the values of a_i , b_i , and c_i , the triangle-shaped functions change consequently, and thus represent different forms of membership functions on the linguistic label A_i . Any piecewise and continuous differentiable functions are eligible to be node functions. These parameters are referred to as premise parameters.

Layer 2: Each node in this layer, indicated by a circle node tagged Π , multiplies the entering signals and sends the product out:

$$O_i^2 = w_i = \mu_{A_i}(x)\mu_{B_i}(y). \quad (14)$$

Therefore, each node output indicates the firing strength of a rule.

Layer 3: Each node in this layer, indicated by a circle node tagged N , computes the ratio of the i th rule's firing strength to the sum of all rules' firing strengths:

$$O_i^3 = \bar{w}_i = \frac{w_i}{w_1 + w_2}. \quad (15)$$

The outputs of this layer are called normalized firing strengths.

Layer 4: Each node in this layer, indicated by a square node, calculates the contribution of the i th rule to the whole output:

$$O_i^4 = \bar{w}_i f_i = \bar{w}_i(p_i x + q_i y + r_i), \quad (16)$$

where \bar{w}_i is the output of layer 3 and p_i , q_i , and r_i comprise the parameter set. This layer's parameters are referred to as consequent parameters.

Layer 5: The single node, indicated by a circle node, calculates the final output as the summation of all entering signals:

$$O_i^5 = \text{overall_output} = \sum \bar{w}_i f_i = \frac{\sum_i w_i f_i}{\sum_i w_i}. \quad (17)$$

As can be seen in the suggested ANFIS structure (Fig. 2b), the overall output, i.e., f , can be represented by a linear combination of the consequent parameters:

$$\begin{aligned} f &= \frac{w_1}{w_1 + w_2} f_1 + \frac{w_2}{w_1 + w_2} f_2 \\ &= \bar{w}_1 f_1 + \bar{w}_2 f_2 \\ &= (\bar{w}_1 x) p_1 + (\bar{w}_1 y) q_1 + \bar{w}_1 r_1 \\ &\quad + (\bar{w}_2 x) p_2 + (\bar{w}_2 y) q_2 + \bar{w}_2 r_2. \end{aligned} \quad (18)$$

As can be seen in Fig. 3, the membership functions of the input variables represent seven sets. The rule table and the membership function boundaries for both subsystems presented in Table 2 are similarly selected.

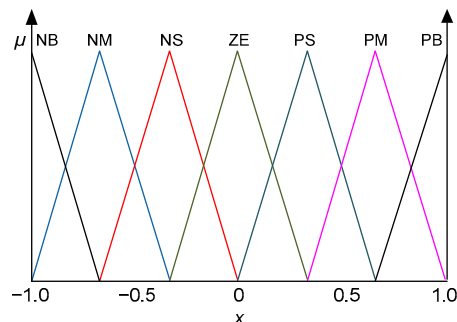


Fig. 3 Normalized membership function for inputs (References to color refer to the online version of this figure)

Table 2 Look up table of fuzzy rules

$\frac{\Delta\dot{\omega}}{\Delta\dot{P}}$	$\frac{\Delta\omega/\Delta u}{\Delta\omega/\Delta u}$						
	NB	NM	NS	ZE	PS	PM	PB
NB	NB	NB	NB	NB	NM	NS	ZE
NM	NB	NM	NM	NM	NS	ZE	PS
NS	NB	NM	NS	NS	ZE	PS	PM
ZE	NB	NM	NS	ZE	PS	PM	PB
PS	NM	NS	ZE	PS	PS	PM	PB
PM	NS	ZE	PS	PM	PM	PM	PB
PB	ZE	PS	PM	PB	PB	PB	PB

4 Hierarchical fuzzy-rule-based system

In a hierarchical fuzzy system, the total number of rules is reduced by reconstructing the fuzzy rules into hierarchical, simple fuzzy subsystems. In this strategy, the modulation process is hierarchically carried out from the initial level to the final level (Takagi and Sugeno, 1983; Jang, 1993; Gyugyi *et al.*, 1997; Rojas *et al.*, 2000). In other words, the first level renders an unfuzzified output, subsequently lined up by the second level so that the process can be replicated in following levels. Fig. 4a shows the general structure of HFRBS with N input variables and Fig. 4b shows classical FRBS with N input variables. It is considered that M membership functions are used to fuzzify each input variable, and the total number of rules can be presented as follows:

$$M^N \text{ rules in a conventional FRBS.} \quad (19)$$

$$M^2(N-1) \text{ rules in a hierarchical FRBS.} \quad (20)$$

A neoteric model of hierarchical fuzzy structure based on the ANFIS controller, i.e., HANFISC-TCSC (Fig. 5), is suggested to enhance the dynamic performance of TCSC. By using this hierarchical structure, the controller's performance is enhanced without exponentially growing the rule table. As shown, this structure is composed of two ANFIS subsystems, and each subsystem is fed by two inputs.

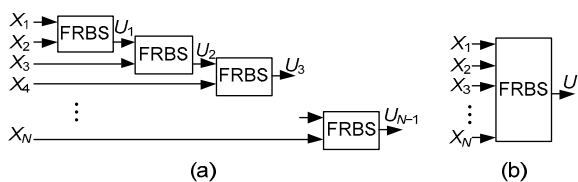


Fig. 4 Hierarchical fuzzy structure (a) and conventional FLC structure method (b)

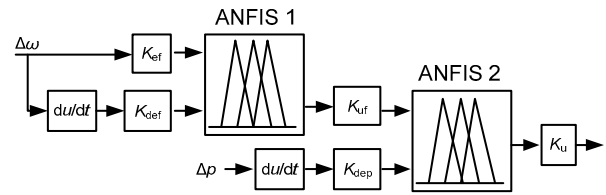


Fig. 5 Construction of the proposed HANFISC-TCSC

5 Linearized model of interconnected multi-area multi-source power systems with HANFISC-TCSC

5.1 Linearization of TCSC relevant to AGC

TCSC is one of the series FACTS families that have been commonly used in transmission lines to control the power flow via compensation of transmission line's reactance. Generally, it is constructed by a series compensating capacitor shunted by a TCR, whose reactance is adjusted by firing the bidirectional thyristor. Also, the reactance of the TCSC can be expressed by a net equivalent reactance (X_{TCSC}), and its relevant compensation can be obtained by operating it either in capacitive or inductive mode (Li *et al.*, 2000; del Rosso *et al.*, 2003; Falehi, 2012). Fig. 6 shows a single-line diagram of an interconnected multi-area power system of two areas with the studied TCSC located in series with the tie-line to carry out the linearization process. Because of the trivial resistance of the tie-line with respect to the inductance of the tie-line, it is neglected in an acceptable approximation. Anyhow, TCSC can be used to suppress the area frequency oscillations by controlling the tie-line power quickly.

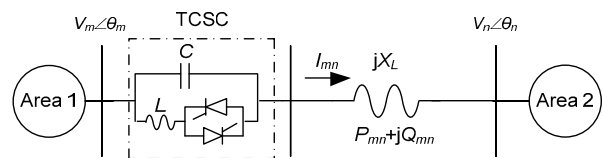


Fig. 6 Single-line diagram of a two-area interconnected multi-area power system with series-connected TCSC

With the TCSC located in series with the tie-line, the flow of current from area m to area n can be formulated as

$$I_{mn} = \frac{V_m \angle \theta_m - V_n \angle \theta_n}{j(X_L - X_{TCSC})}. \quad (21)$$

Also, the flow of power from bus m to bus n is

$$S_{mn} = V_m I_{mn}^* = P_{mn} + jQ_{mn}. \quad (22)$$

By extracting the real component of Eq. (22), we obtain

$$P_{mn} = \frac{V_m V_n}{X_L - X_{TCSC}} \sin(\theta_m - \theta_n). \quad (23)$$

Let k_c denote the rate of compensation by TCSC, i.e., $k_c = X_{TCSC}/X_L$. Eq. (23) can be represented by

$$P_{mn} = \frac{V_m V_n}{X_L(1 - k_c)} \sin(\theta_m - \theta_n). \quad (24)$$

Provided Eq. (24) is linearized, the relationship of the active power flow can be written as

$$\Delta P_{mn} = \frac{V_m V_n}{X_L(1 - k_c^0)^2} \sin(\theta_m^0 - \theta_n^0) \Delta k_c + \frac{V_m V_n}{X_L(1 - k_c^0)} \cos(\theta_m^0 - \theta_n^0) (\Delta \theta_m - \Delta \theta_n). \quad (25)$$

Let T_{mn}^0 denote the synchronizing coefficient:

$$T_{mn}^0 = \frac{V_m V_n}{X_L} \cos(\theta_m^0 - \theta_n^0),$$

and also

$$J_{mn}^0 = \frac{V_m V_n}{X_L} \sin(\theta_m^0 - \theta_n^0).$$

Then, Eq. (25) can be written as

$$\Delta P_{mn} = \frac{J_{mn}^0}{(1 - k_c^0)^2} \Delta k_c + \frac{T_{mn}^0}{1 - k_c^0} (\Delta \theta_m - \Delta \theta_n). \quad (26)$$

Since $\Delta \theta_m = \int \Delta \omega_m dt$ and $\Delta \theta_n = \int \Delta \omega_n dt$, the Laplace transform of Eq. (26) is

$$\Delta P_{mn}(s) = \frac{J_{mn}^0}{(1 - k_c^0)^2} \Delta k_c(s) + \frac{T_{mn}^0}{s(1 - k_c^0)} (\Delta \omega_m(s) - \Delta \omega_n(s)). \quad (27)$$

According to Eq. (27), the flow of tie-line power can be controlled by $\Delta k_c(s)$, i.e., by regulating the rate of compensation (X_{TCSC}). The relevant controller to modify the TCSC equivalent reactance can be given by the following transfer function:

$$\Delta k_c(s) = \frac{1 + T_1 s}{1 + T_2 s} \frac{1 + T_3 s}{1 + T_4 s} \frac{K_{TCSC}}{1 + s T_{TCSC}} \Delta \omega_m(s), \quad (28)$$

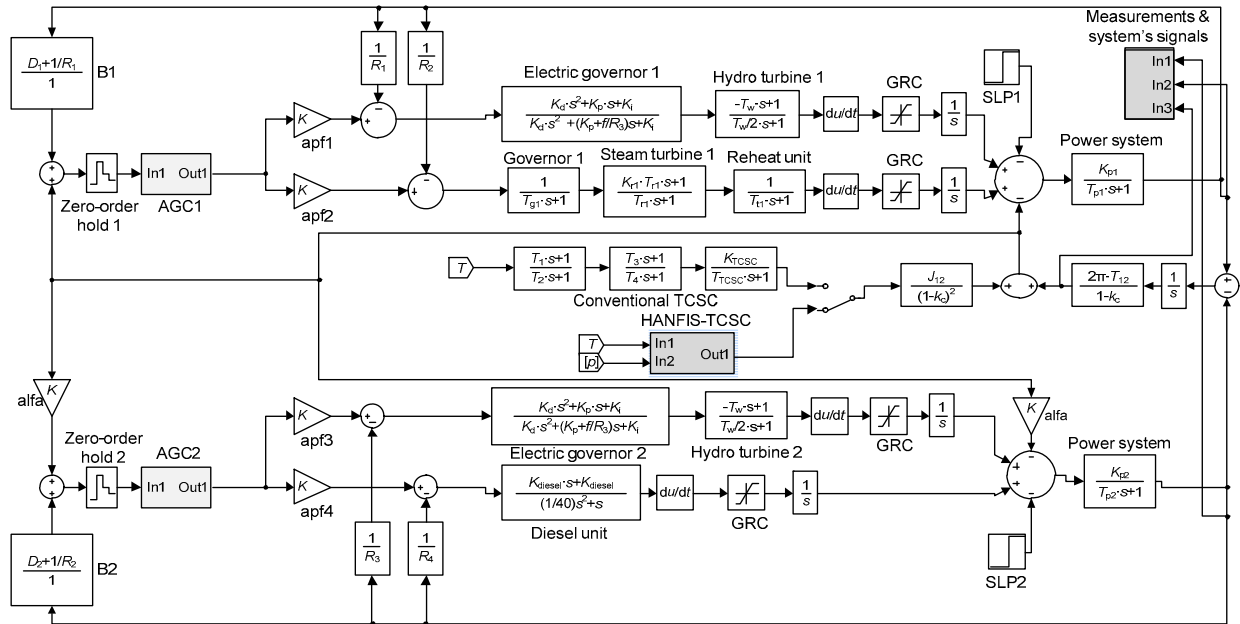
where K_{TCSC} and T_{TCSC} are the gain and time constant of the TCSC controller, respectively, and T_1 , T_2 , T_3 , and T_4 are time constants of lead lag phase compensation blocks.

According to Eq. (28), $\Delta \omega(s)$ can be used as the control signal of TCSC to adjust X_{TCSC} and regulate the flow of tie-line power between two areas and subsequently suppress the dynamic oscillations of tie-line power exchanges and frequency. Thus,

$$\Delta P_{mn}(s) = \frac{J_{mn}^0}{(1 - k_c^0)^2} \frac{1 + T_1 s}{1 + T_2 s} \frac{1 + T_3 s}{1 + T_4 s} \frac{K_{TCSC}}{1 + s T_{TCSC}} \Delta \omega_m(s) + \frac{T_{mn}^0}{s(1 - k_c^0)} (\Delta \omega_m(s) - \Delta \omega_n(s)). \quad (29)$$

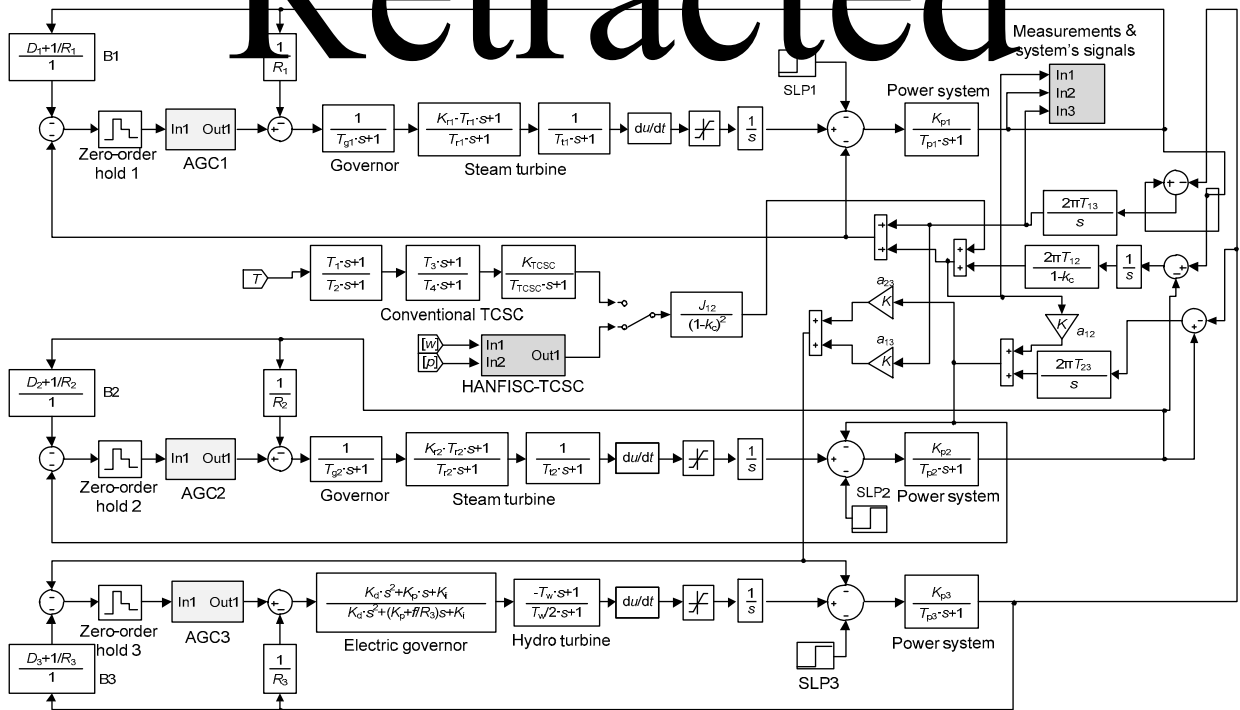
5.2 Linearized model of a two-area hydro-thermal-diesel power system

As has already been pointed out, AGC can track and control only normal load changes that are slow and small. Hence, the nonlinear dynamical equations of the power system must be linearized during small load changes around an operating point. A schematic of a linearized interconnected power system with a TCSC in series with the tie-line is presented in Fig. 7a. The generation rate constraint (GRC) is considered 10%/min for the thermal area, and 270%/min for raising generation and 360%/min for lowering generation in the hydro area. The power system has two generating areas with different capacities (area 1, 1800 MW and area 2, 1200 MW). Both areas consist of two hydro generation units. The other relevant parameters are given in Appendix A.



(a)

Retracted



(b)

Fig. 7 Linearized model of a two-area hydro-thermal-diesel power system (a) and linearized model of a three-area hydro-thermal power system (b)

5.3 Linearized model of a three-area hydro-thermal power system

The power system under study with the presence of TCSC has been constructed by three equal generating areas: two reheat thermal system for areas 1 and 2, and a hydro system for area 3 (Fig. 7b). The characteristics of the steam turbine differ from those of the hydro turbine in many respects. GRC is considered 3%/min in thermal areas, and 270%/min (4.5%/s) for raising and 360%/min (6%/s) for lowering generation in the hydro area. This power system has been constructed by three equal generating areas with 2000 MW capacity. A bias setting of B_i is chosen for both thermal and hydro areas. The other relevant parameters are given in Appendix B.

5.4 Multi-area multi-source interconnected power systems with the presence of HANFISC-TCSC

Naughting the area control error (ACE) of each area of an interconnected power system has been formulated as the main aim of the AGC system. The system frequency and tie-line power exchange deviations are the two primary and fundamental criteria regarding ACE, which can be stated as follows (Goshal, 2004; Divya and Nagendra Rao, 2005):

$$ACE_i = \sum_j \Delta p_{tie,i,j} + B_i \Delta f_i, \quad (30)$$

where $\Delta p_{tie,i,j}$ is the tie-line power deviation between the i th area and the j th area, B_i is the frequency bias coefficient of the i th area, and Δf_i is the frequency error of the i th area.

As has already been stated, HANFISC-TCSC is suggested in place of AGC, aiming at augmenting the overall dynamic performance of both interconnected power systems. In the meantime, a conventional MOPSO-TCSC has been tested and evaluated along with the suggested structure to clarify its high dynamic performance. In this regard, the related parameters that should be optimally tuned by MOPSO are:

1. HANFISC-TCSC: K_{ef} , K_{def} , K_{uf} , K_{dep} , and K_u .
2. Conventional TCSC: K_{TCSC} , T_{TCSC} , T_1 , and T_3 .

The values of T_2 and T_4 are taken as 0.1.

5.5 Objective functions

Hitherto, a number of techniques have been used

to evaluate the performance of a control system, including the integral time-weighted absolute error (ITAE), integral time-weighted squared error (ITSE), integral squared error (ISE), and integral absolute error (IAE). In spite of that, an effective strategy has been executed for the simultaneous optimal adjustment of both the controllers, aimed at clarifying the high efficiency of HANFISC-TCSC compared to the conventional MOPSO-TCSC. This relationship is indicated by the following functions (Falehi and Rostami, 2011; Falehi, 2013):

$$J_f = \int_{t=0}^{t=t_{sim}} \sum |\Delta f_i| dt, \quad (31)$$

$$J_p = \int_{t=0}^{t=t_{sim}} \sum |\Delta p_{tie,i,j}| dt, \quad (32)$$

$$F_f = \sum_{k=1}^{N_p} J_{f,k}, \quad (33)$$

$$F_p = \sum_{k=1}^{N_p} J_{p,k}, \quad (34)$$

where N_p and t_{sim} are the number of SLPs and simulation time period, respectively, J_f and J_p are two prominent benchmarks controlling the system stability, and F_f and F_p are the suggested functions related to carrying out the simultaneous optimal scheme to mitigate the low-frequency power oscillations and the tie-line power exchange deviations, respectively. Eventually, the problem is formulated as the following optimization problem:

$$\min F_f \text{ and } F_p. \quad (35)$$

A flowchart of the optimization problem based on simultaneous adjustment by considering a 2% SLP in all areas of both power systems is shown in Fig. 8.

6 Simulation results

6.1 Two-area hydro-thermal-diesel power system

To corroborate the performance of HANFISC-TCSC by performing the simultaneous optimal tuning scheme, the power system has been affected by a 2% SLP condition in both areas. This optimization strategy has been carried out for both HANFISC-TCSC and conventional MOPSO-TCSC by appraising the

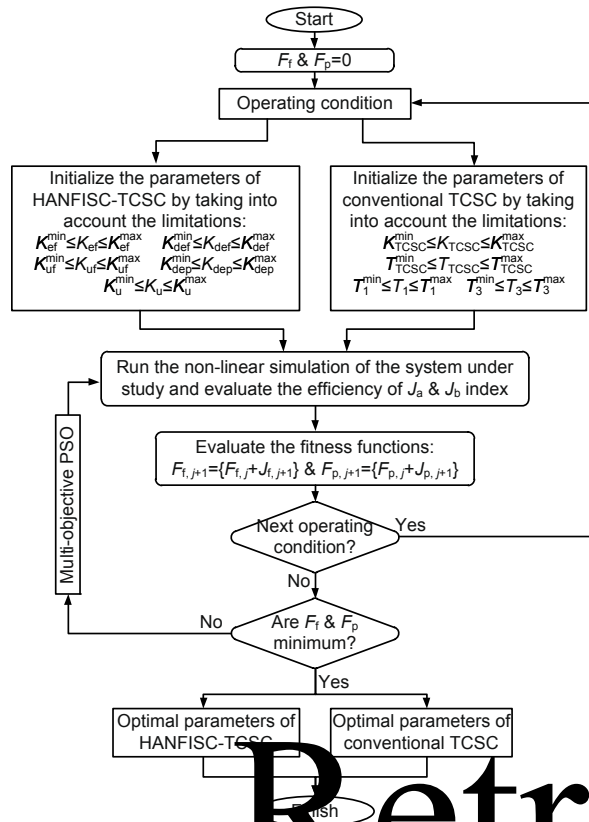


Fig. 8 Simultaneous optimization scheme based on multi-objective particle swarm

proposed fitness function regarding two SLP conditions. Optimal parameters of both controllers are accordingly tabulated in Tables 3 and 4. Meanwhile, the eigenvalue analyses in the presence of both HANFISC-TCSC and conventional MOPSO-TCSC are depicted in Fig. 9. It is obvious that the power system stability is better when HANFISC-TCSC is incorporated in the power system as compared to the conventional MOPSO-TCSC.

Table 3 Optimum parameters of the two-area hydro-thermal-diesel power system’s HANFISC-TCSC

K_{ef}	K_{def}	K_{uf}	K_{dep}	K_u
38.8478	1.77953	2.48272	17.6579	39.2464

Table 4 Optimum parameters of the two-area hydro-thermal-diesel power system’s conventional MOPSO-TCSC

K_{TCSC}	T_{TCSC}	T_1	T_3
0.37237	0.51803	0.38512	0.55979

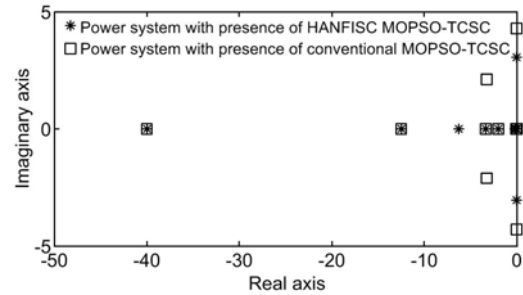


Fig. 9 Eigenvalues of a two-area hydro-thermal-diesel power system with both controllers

In the long term, the high performance of HANFISC-TCSC aimed at augmentation of the power system’s dynamic stability has been revealed by the results in the following sections.

6.1.1 Perturbation in area 1

In this part of the study, a 2% SLP takes place at $t=10$ s in area 1 to evaluate the performance of the suggested controller. As described above, the optimization scheme based on MOPSO undertakes the simultaneous optimization of the controllers’ parameters. The system response presented in Fig. 10 have confirmed the above-mentioned conclusion.

6.1.2 Perturbation in area 2

For this state, it is considered that a 3% SLP impacted the power system at $t=10$ s in area 2 to evaluate the performance of the proposed controller. Similar to the previous case, after performing the optimization scheme, the system response obtained has confirmed the high dynamic performance of HANFISC-TCSC (Fig. 11).

6.2 Three-area hydro-thermal power system

The effectiveness and robustness of HANFIS-TCSC has been thoroughly evaluated to augment the power system’s dynamic stability with regard to a 3% SLP, which is triggered at $t=10$ s in all areas of this power system. The response of the affected power system has been dealt with and analyzed employing both controllers. After unraveling the optimization problem, the optimum parameters of HANFIS-TCSC and conventional MOPSO-TCSC were evaluated (Tables 5 and 6).

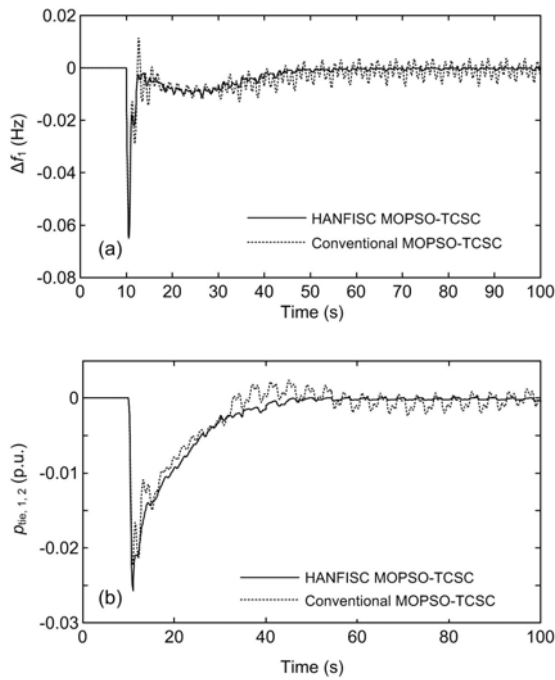


Fig. 10 Power system responses under a 2% SLP in area 1 at $t=10$ s: (a) frequency error of the first area; (b) tie-line power deviation between the first and the second areas

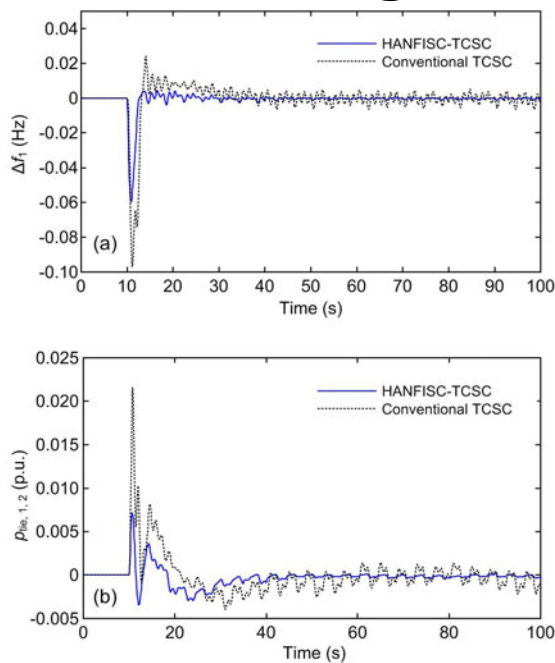


Fig. 11 Power system responses under a 3% SLP in area 2 at $t=10$ s: (a) frequency error of the first area; (b) tie-line power deviation between the first and the second areas

Table 5 Optimal parameters of the hydro-thermal power system's HANFISC-TCSC

K_{ef}	K_{def}	K_{uf}	K_{dep}	K_u
1.1372	0.9866	1.4796	0.75322	0.015271

Table 6 Optimal parameters of the hydro-thermal power system's conventional MOPSO-TCSC

K_{TCSC}	T_{TCSC}	T_1	T_3
0.26983	0.35560	0.29761	0.40645

The Pareto solution front of the optimization problem is shown in Fig. 12. The eigenvalue analyses in presence of both HANFISC-TCSC and the conventional MOPSO-TCSC are presented in Fig. 13. The results presented here precisely show more stability of the power system using HANFISC-TCSC as compared to the power system with the conventional MOPSO-TCSC.

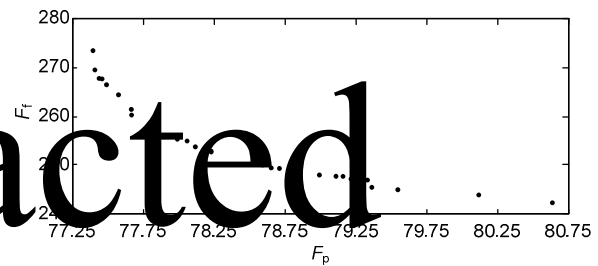


Fig. 12 Pareto front extracted from objective functions of a three-area hydro-thermal power system

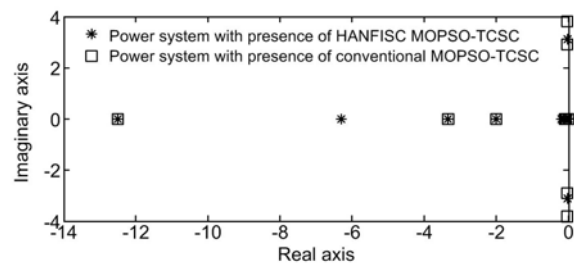


Fig. 13 Eigenvalues of a three-area hydro-thermal power system with both controllers

HANFISC-TCSC has displayed and proved its high dynamic performance, as shown in the following sections (Figs. 14–16).

6.2.1 Perturbation in area 1

For this section, we consider a 3% SLP to be occurring at $t=10$ s in area 1, and we appraise the dynamic performance of both controllers. As previously mentioned, the simultaneous optimization

scheme based on MOPSO has been carried out to tune the controllers' parameters considering the occurrence of perturbation in each area of this power system. The system response is presented in Fig. 14. The represented curves have transparently corroborated above-mentioned citation. Here, as in Section 5.1, all criteria of stability, including overshoot, undershoot, settling time, steady-state error of tie-line power, and frequency exchanges significantly decrease with HANFISC-TCSC compared with the conventional MOPSO-TCSC. It can be said that HANFISC-TCSC has significantly enhanced the dynamic stability of the power system.

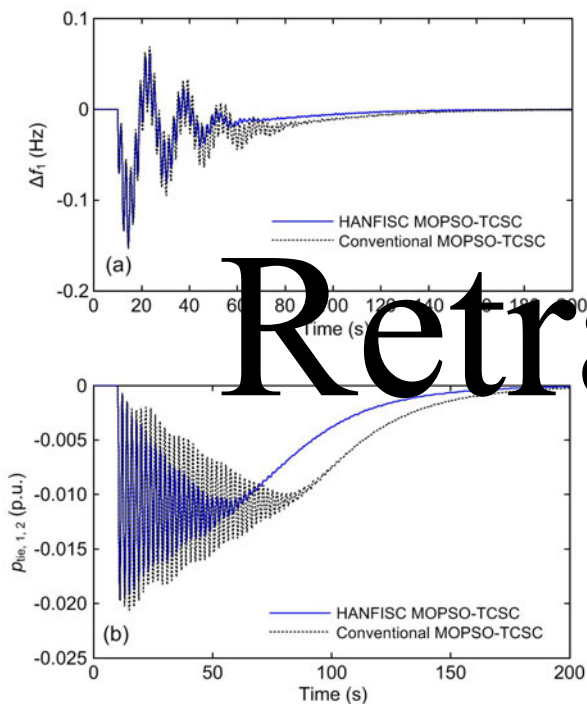


Fig. 14 Power system responses under a 3% SLP in area 1 at $t=10$ s: (a) frequency error of the first area; (b) tie-line power deviation between the first and second areas

6.2.2 Perturbation in area 2

Similar to the previous case, the power system is assumed to be affected by a 4% SLP in area 2 at $t=10$ s and we evaluate the dynamic performance of HANFISC-TCSC and the conventional MOPSO-TCSC, respectively, in dealing with this situation (Fig. 15). As expected, the power system's dynamic oscillations have been impressively alleviated by the proposed controller compared to the conventional MOPSO-TCSC.

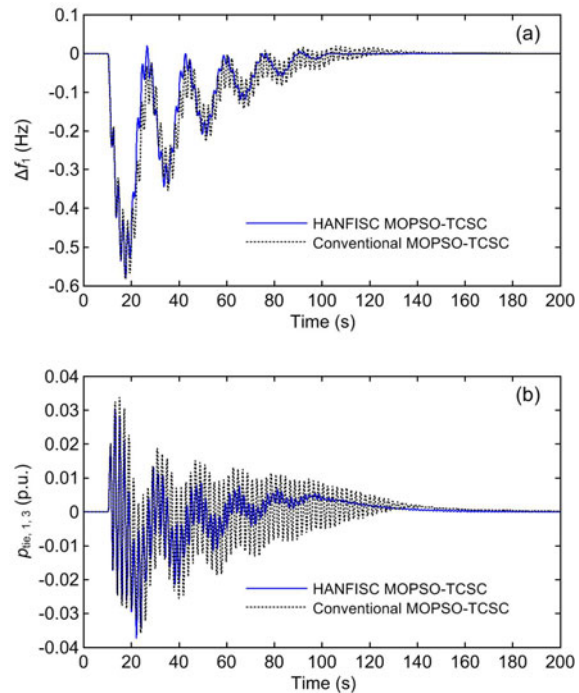


Fig. 15 Power system responses under a 4% SLP in area 2 at $t=10$ s: (a) frequency error of the first area; (b) tie-line power deviation between the first and third areas

Retracted

6.2.3 Perturbation in area 3

For this part of study, a 5% SLP is assumed to impact the power system at $t=10$ s in area 3, and we appraise the dynamic performance of HANFISC-TCSC. As can be seen from Fig. 16, the dynamic stability of the power system has been significantly enhanced by the proposed controller.

7 Conclusions

In this paper, we proposed a high-performance HANFISC-TCSC to rapidly bring the affected interconnected multi-area power system to the stable status. For this, the alleviation of the two prominent issues, i.e., low-frequency power oscillations and tie-line power exchange deviations, has been formulated as a multi-objective optimization problem. Meanwhile, MOPSO was chosen to solve the problem under study. Two different multi-area multi-source interconnected power systems, i.e., two-area hydro-thermal-diesel and three-area hydro-thermal power systems, have been considered to provide an

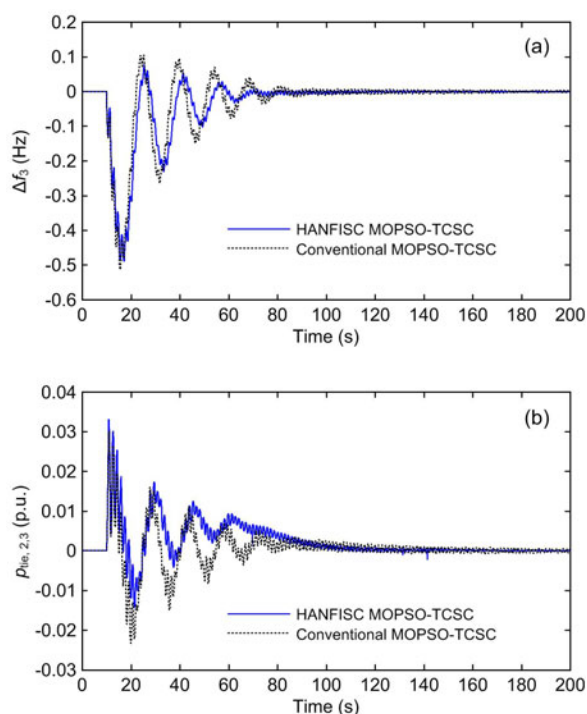


Fig. 16 Power system responses under a 5% SLP in area 3 at $t=10$ s: (a) frequency error of the third area; (b) tie-line power deviation between the second and third areas

appropriate setting to evaluate the dynamic performance of HANFISC-TCSC. In the interim, the capability of HANFISC-TCSC has been perfectly evaluated along with the conventional MOPSO-TCSC with regard to the incidence of SLP in all areas of both test power systems. Simulations results from both multi-area interconnected power systems have conclusively proved the high dynamic performance of the proposed HANFISC-TCSC in comparison with the conventional MOPSO-TCSC.

References

- Abd-Elazim, S.M., Ali, E.S., 2016. Load frequency controller design via BAT algorithm for nonlinear interconnected power system. *Int. J. Electr. Power Energy Syst.*, **77**:166-177. <http://dx.doi.org/10.1016/j.ijepes.2015.11.029>
- Abd-Elaziz, A.Y., Ali, E.S., 2015. Cuckoo search algorithm based load frequency controller design for nonlinear interconnected power system. *Int. J. Electr. Power Energy Syst.*, **73**:632-643. <http://dx.doi.org/10.1016/j.ijepes.2015.05.050>
- Ali, E.S., Abd-Elazim, S.M., 2011. Bacteria foraging optimization algorithm based load frequency controller for interconnected power system. *Int. J. Electr. Power Energy Syst.*, **33**(3):633-638. <http://dx.doi.org/10.1016/j.ijepes.2010.12.022>

- Ali, E.S., Abd-Elazim, S.M., 2013. BFOA based design of PID controller for two area load frequency control with nonlinearities. *Int. J. Electr. Power Energy Syst.*, **51**:224-231. <http://dx.doi.org/10.1016/j.ijepes.2013.02.030>
- Benabid, R., Boudour, M., Abido, M.A., 2009. Optimal location and setting of SVC and TCSC devices using non-dominated sorting particle swarm optimization. *Electr. Power Syst. Res.*, **79**(12):1668-1677. <http://dx.doi.org/10.1016/j.epr.2009.07.004>
- Benitez, A.D., Casillas, J., 2013. Multi-objective genetic learning of serial hierarchical fuzzy systems for large-scale problems. *Soft Comput.*, **17**(1):165-194. <http://dx.doi.org/10.1007/s00500-012-0909-2>
- Bevrani, H., Hiyama, T., Mitani, Y., 2008. Power system dynamic stability and voltage regulation enhancement using an optimal gain vector. *Contr. Eng. Pract.*, **16**(9):1109-1119. <http://dx.doi.org/10.1016/j.conengprac.2008.01.001>
- Cai, L., Erlich, I., 2005. Simultaneous coordinated tuning of PSS and FACTS damping controllers in large power systems. *IEEE Trans. Power Syst.*, **20**(1):294-300. <http://dx.doi.org/10.1109/TPWRS.2004.841177>
- Chaudhuri, B., Pal, B., 2004. Robust damping of multiple swings modes employing global stabilizing signals with TCSC. *IEEE Trans. Power Syst.*, **19**(1):499-506. <http://dx.doi.org/10.1109/TPWRS.2003.821463>
- Chaudhuri, B., Pal, B., Zlotar, A.C., 2003. Mixed-sensitivity approach to H_2 control of power system oscillations employing multiple FACTS devices. *IEEE Trans. Power Syst.*, **18**(3):1149-1156. <http://dx.doi.org/10.1109/TPWRS.2003.811311>
- Dash, P.K., Morris, S., Mishra, S., 2004. Design of a nonlinear variable-gain fuzzy controller for FACTS devices. *IEEE Trans. Contr. Syst. Technol.*, **12**(3):428-438. <http://dx.doi.org/10.1109/TCST.2004.824332>
- del Rosso, A.D., Canizares, C.A., Dona, V.M., 2003. A study of TCSC controller design for power system stability improvement. *IEEE Trans. Power Syst.*, **18**(4):1487-1496. <http://dx.doi.org/10.1109/TPWRS.2003.818703>
- Divya, K.C., Nagendra Rao, P.S., 2005. A simulation model for AGC studies of hydro-hydro systems. *Int. J. Electr. Power Energy Syst.*, **27**(5-6):335-342. <http://dx.doi.org/10.1016/j.ijepes.2004.12.004>
- Eberhart, R.C., Shi, Y.H., Kennedy, J., 2001. *Swarm Intelligence*. Academic Press, San Diego, CA.
- Elshafei, A.L., El-Metwally, K.A., Shaltout, A.A., 2005. A variable-structure adaptive fuzzy-logic stabilizer for single and multi-machine power systems. *Contr. Eng. Pract.*, **13**(4):413-423. <http://dx.doi.org/10.1016/j.conengprac.2004.03.017>
- Falehi, A.D., 2012. Simultaneous coordinated design of TCSC-based damping controller and AVR based on PSO technique. *Electr. Rev.*, **88**(5):136-140.
- Falehi, A.D., 2013. Design and scrutiny of maiden PSS for alleviation of power system oscillations using RCGA and PSO techniques. *J. Electr. Eng. Technol.*, **8**(3):402-410.

- <http://dx.doi.org/10.5370/JEET.2013.8.3.402>
- Falehi, A.D., Rostami, M., 2011. Design and analysis of a novel dual-input PSS for damping of power system oscillations employing RCGA-optimization technique. *Int. Rev. Electr. Eng.*, **6**(2):938-945.
- Falehi, A.D., Dankoob, A., Amirkhan, S., *et al.*, 2011. Coordinated design of STATCOM-based damping controller and dual-input PSS to improve transient stability of power system. *Int. Rev. Electr. Eng.*, **6**(3):1308-1318.
- Falehi, A.D., Rostami, M., Doroudi, A., *et al.*, 2012. Optimization and coordination of SVC-based supplementary controllers and PSSs to improve the power system stability using genetic algorithm. *Turk. J. Electr. Eng. Comput. Sci.*, **20**(5):639-654. <http://dx.doi.org/10.3906/elk-1010-838>
- Goshal, S.P., 2004. Optimization of PID gains by particle swarm optimization in fuzzy based automatic generation control. *Electr. Power Syst. Res.*, **72**(3):203-212. <http://dx.doi.org/10.1016/j.epsr.2004.04.004>
- Gyugyi, L., 1992. Unified power-flow control concept for flexible AC transmission systems. *IEE Proc. C*, **139**(4): 323-331. <http://dx.doi.org/10.1049/ip-c.1992.0048>
- Gyugyi, L., Schauder, C.D., Sen, K.K., 1997. Static synchronous series compensator: a solid-state approach to the series compensation of transmission lines. *IEEE Trans Power Del.*, **12**(1):40-41. <http://dx.doi.org/10.1109/69.568265>
- Hingorani, N.G., Gyugyi, L., 2000. Understanding FACTS: Concepts and Technology of Flexible AC Transmission Systems. IEEE Press, New York.
- Iraclous, D.P., Alexandridis, A.T., 2005. A multi-task automatic generation control for power regulation. *Electr. Power Syst. Res.*, **73**(3):275-285. <http://dx.doi.org/10.1016/j.epsr.2004.06.011>
- Jang, J.S.R., 1993. ANFIS: adaptive-network-based fuzzy inference system. *IEEE Trans. Syst. Man Cybern.*, **23**(3):665-685. <http://dx.doi.org/10.1109/21.256541>
- Karnavas, Y.L., Papadopoulos, D.P., 2000. Excitation control of a power-generating system based on fuzzy logic and neural networks. *Int. Trans. Electr. Energy Syst.*, **10**(4): 233-241. <http://dx.doi.org/10.1002/etep.4450100406>
- Kazemi, A., Jahed Motlagh, M.R., Naghshbandy, A.H., 2007. Application of a new multi-variable feedback linearization method for improvement of power systems transient stability. *Int. J. Electr. Power Energy Syst.*, **29**(4): 322-328. <http://dx.doi.org/10.1016/j.ijepes.2006.07.011>
- Kikuchi, H., Otake, A., Nakanishi, S., 1998. Functional completeness of hierarchical fuzzy modeling. *Inform. Sci.*, **110**(1-2):51-60. [http://dx.doi.org/10.1016/S0020-0255\(97\)10076-7](http://dx.doi.org/10.1016/S0020-0255(97)10076-7)
- Kundur, P., Klein, M., Rogers, G.J., *et al.*, 1989. Application of power system stabilizers for enhancement of overall system stability. *IEEE Trans. Power Syst.*, **4**(2):614-626. <http://dx.doi.org/10.1109/59.193836>
- Larsen, E.V., Sanchez-Gasca, J.J., Chow, J.H., 1995. Concepts of design of FACTS controllers to damp power swings. *IEEE Trans. Power Syst.*, **10**(2):948-956. <http://dx.doi.org/10.1109/59.387938>
- Lee, M.L., Chung, H.Y., Yu, F.M., 2003. Modeling of hierarchical fuzzy systems. *Fuzzy Sets Syst.*, **138**(2):343-361. [http://dx.doi.org/10.1016/S0165-0114\(02\)00517-1](http://dx.doi.org/10.1016/S0165-0114(02)00517-1)
- Li, B.H., Wu, Q.H., Turner, D.R., *et al.*, 2000. Modeling of TCSC dynamics for control and analysis of power system stability. *Int. J. Electr. Power Energy Syst.*, **22**(1):43-49. [http://dx.doi.org/10.1016/S0142-0615\(99\)00037-X](http://dx.doi.org/10.1016/S0142-0615(99)00037-X)
- Mattavelli, P., Verghese, G.C., Stankovic, A.M., 1997. Phasor dynamics of thyristor-controlled series capacitor systems. *IEEE Trans. Power Syst.*, **12**(3):1259-1267. <http://dx.doi.org/10.1109/59.630469>
- Moradi, A., Shirazi, K.H., Keshavarz, M., *et al.*, 2014. Smart piezoelectric patch in non-linear beam: design, vibration control and optimal location. *Trans. Instit. Meas. Contr.*, **36**(1):131-144. <http://dx.doi.org/10.1177/0142331213495041>
- Panda, S., Padhy, N.P., 2008. Comparison of particle swarm optimization and genetic algorithm for FACTS-based controller design. *Appl. Soft Comput.*, **8**(4):1418-1427. <http://dx.doi.org/10.1016/j.asoc.2007.10.009>
- Raju, G., Zhou, J., Kisner, R., 1991. Hierarchical fuzzy control. *Int. J. Contr.*, **54**(5):1201-1216. <http://dx.doi.org/10.1080/00207179108934205>
- Rojas, L., Benjfer, J.J., Rodriguez Alvarez, R., *et al.*, 2000. What are the main functional blocks involved in the design of adaptive neuro-fuzzy inference systems? IEEE-INNS-ENNS Int. Joint Conf. on Neural Networks, p.551-556. <http://dx.doi.org/10.1109/IJCNN.2000.859453>
- Soliman, H.M., Dabroum, A., Mahmoud, M.S., *et al.*, 2011. Guaranteed-cost reliable control with regional pole placement of a power system. *J. Franklin Instit.*, **348**(5): 884-898. <http://dx.doi.org/10.1016/j.jfranklin.2011.02.013>
- Takagi, T., Sugeno, M., 1983. Derivation of fuzzy control rules from human operator's control actions. IFAC Symp. on Fuzzy Information, Knowledge Representation and Decision Analysis, p.55-60.
- Talaat, H.E.A., Abdennour, A., Al-Sulaiman, A.A., 2010. Design and experimental investigation of a decentralized GA-optimized neuro-fuzzy power system stabilizer. *Int. J. Electr. Power Energy Syst.*, **32**(7):751-759. <http://dx.doi.org/10.1016/j.ijepes.2010.01.011>
- Tan, W., Xu, Z., 2009. Robust analysis and design of load frequency controller for power systems. *Electr. Power Syst. Res.*, **79**(5):846-853. <http://dx.doi.org/10.1016/j.epsr.2008.11.005>
- Zhang, Y., Zhou, Q., Sun, C.X., *et al.*, 2008. RBF neural network and ANFIS-based short-term load forecasting approach in real-time price environment. *IEEE Trans. Power Syst.*, **23**(3):853-858. <http://dx.doi.org/10.1109/TPWRS.2008.922249>

Appendix A: Relevant parameters of the two-area hydro-thermal-diesel power system

$K_{p1}=K_{p2}=120$ Hz/p.u. MW, $R_1=R_2=R_3=R_4=2.4$ Hz/p.u. MW, $T_g=0.08$ s, $T_t=0.3$ s, $T_r=5$ s, $T_w=1$ s, $K_p=1.0$, $K_i=5.0$, $K_d=4.0$, $D_i=0.00833$ p.u. MW/Hz, $P_{R1}=1800$ MW, and $P_{R2}=1200$ MW.

Appendix B: Relevant parameters of the three-area hydro-thermal power system

$f=60$ Hz, $T_{gi}=0.08$ s, $T_{ri}=10$ s, $H_i=5$ s, $T_{ti}=0.3$ s, $K_r=0.5$, $P_{ri}=2000$ MW, $T_{pi}=20$ s, $K_d=4.0$, $K_p=1.0$, $K_i=5.0$, $D_i=0.1283$ p.u. MW/Hz, $K_{pi}=120$ Hz/p.u. MW, $T_w=1$ s.

Retracted